Journal of Solid State Chemistry 181 (2008) 2808–2813

Contents lists available at ScienceDirect

Journal of Solid State Chemistry

journal homepage: www.elsevier.com/locate/jssc

Order–disorder in In^{3+} perovskites: The example of $A(In_{2/3}B''_{1/3})O_3$ (A = Ba, Sr; B'' = W, U)

S.A. Larrégola [a,*], J.A. Alonso [b], R.M. Pinacca [a], M.C. Viola [a], J.C. Pedregosa [a]

[a] Departamento de Química, Área de Química General e Inorgánica, Facultad de Química, Bioquímica y Farmacia, Universidad Nacional de San Luis, Chacabuco y Pedernera, 5700 San Luis, Argentina

[b] Instituto de Ciencia de Materiales de Madrid, C.S.I.C., Cantoblanco, 28049 Madrid, Spain

ARTICLE INFO

Article history:
Received 28 April 2008
Received in revised form
19 June 2008
Accepted 20 June 2008
Available online 1 July 2008

Keywords:
Double perovskite
Neutron powder diffraction
X-ray powder diffraction
Rietveld refinement
Anti-site disordering
Uranium

ABSTRACT

We describe the preparation and structural characterization of four In-containing perovskites from neutron powder diffraction (NPD) and X-ray powder diffraction (XRPD) data. $Sr_3In_2B''O_9$ and $Ba(In_{2/3}B''_{1/3})O_3$ (B'' = W, U) were synthesized by standard ceramic procedures. The crystal structure of the W-containing perovskites and $Ba(In_{2/3}U_{1/3})O_3$ have been revisited based on our high-resolution NPD and XRPD data, while for the new U-containing perovskite $Sr_3In_2UO_9$ the structural refinement was carried out from high-resolution XRPD data. At room temperature, the crystal structure for the two Sr phases is monoclinic, space group $P2_1/n$, where the In atoms occupy two different sites $Sr_2[In]_{2d}[In_{1/3}B''_{2/3}]_{2c}O_6$, with $a = 5.7548(2)$ Å, $b = 5.7706(2)$ Å, $c = 8.1432(3)$ Å, $\beta = 90.01(1)^\circ$ for B'' = W and $a = 5.861(1)$ Å, $b = 5.908(1)$ Å, $c = 8.315(2)$ Å, $\beta = 89.98(1)^\circ$ for B'' = U. The two phases with A = Ba should be described in a simple cubic perovskite unit cell (S.G. $Pm\bar{3}m$) with In and B'' distributed at random at the octahedral sites, with $a = 4.16111(1)$ Å and 4.24941(1) Å for W and U compounds, respectively.

1. Introduction

Double perovskites of formula $A_2B'B''O_6$ have been studied very extensively since the discovery of room temperature colossal magnetoresistance in Sr_2FeMoO_6 [1]. Since many years, various appealing properties, such as ferroelectricity [2], antiferroelectricity [3] or magnetoelectric behaviour [4], have been described, showing that this kind of materials are candidate for distinct technological applications in new generation devices. The simplest double perovskite $A_2B'B''O_6$ structure (elpasolite type) can be viewed as a regular arrangement of corner-sharing $B'O_6$ and $B''O_6$ octahedra, alternating along the three directions of the crystal, with the large A cations occupying the voids between the octahedra. Depending on the relative size of the A cations with respect to the B′ and B'' ones, the crystal structure is commonly found to be cubic ($Fm\bar{3}m$), tetragonal ($I4/m$) or monoclinic ($P2_1/n$) [5].

A particular type of double perovskites presents the apparently complex stoichiometry $A_3B'_2B''O_9$ [6–9]. The crystallographic formula of these compounds could be re-written as $A_2B'(B'_{1/3}B''_{2/3})O_6$ similar to $A_2B'B''O_6$ double perovskites. They, thus, display an intrinsic partial disordering over half of the perovskite ($B'_{1/3}B''_{2/3}$) positions.

It is well known that the physical properties of these compounds are strongly correlated with some structural factors, mainly, the order–disorder phenomena between the octahedral sites atoms. The most important structural features that affect the long-range order/disorder of the B-cations are various and well known, such as the charge and ionic radii difference between B-site atoms and its electronic configuration, and the size ratio between A and B atoms [10,11]. In the same way, other alternative methods have been proposed to evaluate the order–disorder relationship in this kind of compounds [12].

In particular, we have recently prepared and studied the magnetic properties of $Sr_3Fe_2B''O_9$ with B'' = Mo, U, Te [7–9] and found ferrimagnetic behaviour below $T_C = 280$ K, 330 K and 717 K, respectively. Our main finding for these compounds is that these intrinsically "disordered" perovskites, containing a random distribution of Fe and Mo, U or Te at the B'' positions, exhibit a strong magnetic scattering on the low-angle Bragg positions of the neutron diffraction pattern, originating upon naturally occurring groups of Fe^{3+} cations in which strong antiferromagnetic (AFM) Fe–O–Fe superexchange interactions are promoted, similar to those existing in the $LaFeO_3$ perovskite.

Nevertheless, the double perovskites with $A_2B'(B'_{1/3}B''_{2/3})O_6$ and $A_2B'B''O_6$ stoichiometry containing trivalent p-block elements like In^{3+} cations have received little attention [13–15]. These

* Corresponding author.
E-mail address: salarreg@unsl.edu.ar (S.A. Larrégola).

0022-4596/$ - see front matter © 2008 Elsevier Inc. All rights reserved.
doi:10.1016/j.jssc.2008.06.047

p-elements are able to form more covalent bonds to O atoms, which may contribute to increase the long-range ordering between the B atoms at the octahedral sites.

In order to gain new information about the preparation and structural data of In^{3+}-containing perovskites and its effect on the order–disorder issue, we have prepared and characterized the double perovskites $A_3In_2B''O_9$ with A = Sr, Ba and B'' = W, U. The W oxides were previously studied from X-ray powder diffraction (XRPD) and TEM techniques, and the crystal structures were described as a mixture of two cubic phases (70% $Pm\bar{3}m$ and 30% $Pm\bar{3}m$) for A = Ba, whereas the structure of the Sr compound was reported as a three-dimensional network of corner-linked $(In,W)O_6$ octahedra, characterized by a orthorhombic distortion (S.G. *Pnma*) containing a single octahedral site, where In and W are fully disordered [13]. In the present paper we report on the results of a high-resolution NPD study, re-examining the true symmetry and space group of the W perovskite, synthesized by the ceramic method, and giving a detailed description of the crystal structure. On the other hand, we have synthesized and characterized a new member of the double perovskites U-containing family $Sr_3In_2UO_9$ and re-examined the structure of $Ba(In_{2/3}U_{1/3})O_3$, which was reported in the 1980s, and described as a cubic double perovskite $Pm\bar{3}m$ [16]. These two structures were refined from high-resolution XRPD data and they turned out to be isotypic to the W perovskites.

2. Experimental

2.1. Synthesis

$A(In_{2/3}B''_{1/3})O_3$ (A = Sr, Ba; B'' = W, U) were obtained as well-crystallized powders by using standard solid-state techniques. As starting materials, $BaCO_3$, $SrCO_3$, In_2O_3, WO_3 and $UO_2(CH_3COO)_2.2H_2O$ were used. They were weighed out in the appropriate metal ratios and well mixed in an agate mortar. The mixtures were calcined at 800 °C for 24 h. Subsequently, the products were treated four times at 1150 °C for 6 h with intermediate regrindings. Finally the samples were calcined at 1500 °C for 8 h until a single $A(In_{2/3}B''_{1/3})O_3$ phase was obtained. All the calcination steps were carried out in platinum crucibles.

2.2. X-ray and neutron diffraction analysis

The initial structural identification and characterization of the samples was carried out by laboratory XRPD (Cu$K\alpha$, $\lambda = 1.5406$ Å). NPD data were collected on the high-resolution powder diffractometer D2B (ILL, Grenoble, France) for the W samples. The high-flux mode was used, with a wavelength of 1.594 Å, selected from a Ge monochromator. About 4 g of sample was placed in a vanadium can; the counting time was 3 h. High-resolution XRPD diagrams were collected in a Rigaku MultiFlex diffractometer using the monochromatic Cu$K\alpha$ radiation in 2θ-steps of 0.02 and 5 s counting time in the range $10° \leqslant 2\theta \leqslant 120°$.

The refinement of the crystal structures was performed by the Rietveld method using the program Fullprof [17]. The peak profile was fitted by a pseudo-Voigt function. The following parameters were refined in the final run for the W-containing perovskites: scale factor, background coefficients, zero-point error, pseudo-Voigt corrected for asymmetry parameters, positional coordinates, isotropic thermal factors and occupancy factors for oxygen atoms. For the U-containing samples the structures were refined from XRPD data, refining the same parameters excepting the oxygen occupancy.

3. Results and discussion

3.1. Ba-containing phases

The indexed XRPD diagrams of $Ba(In_{2/3}B''_{1/3})O_3$ (B'' = W, U) shown in Fig. 1 are characteristics of a perovskite-type structure, and they exhibit no superstructure peaks corresponding to the long-range In/B'' ordering. Minor amounts of $BaB''O_4$ were detected from either XRPD or NPD data; the most intense peaks from the impurity are indicated with stars in Fig. 1.

The structural refinements from the room temperature high-resolution NPD data for $Ba(In_{2/3}W_{1/3})O_3$ (BIW) and from XRPD data for $Ba(In_{2/3}U_{1/3}O_3)$ (BIU) were performed in the $Pm\bar{3}m$ space group (No. 221), with unit-cell parameter similar to the ideal cubic perovskite aristotype $a_0 \approx 4$ Å, where there is no possibility of long-range order between the two cations occupying the B positions. In this model, In and B'' were located at the same crystallographic Wickoff sites (1*a*; 000), Ba atoms were at 1*b* positions ($\frac{111}{222}$) and O atoms at the 3*d*-sites ($\frac{1}{2}00$). In both patterns a minor impurity of $BaB''O_4$ was detected and included in the refinement as a second phase. For the two samples the impurities $BaB''O_4$ were defined in the space group *Pbcm* (no. 57) and from the scale factors, the amount of $BaUO_4$ was 1.35% for the U phase, while for the W sample the amount of $BaWO_4$ was 1.02%. An excellent fit was obtained for both refinements (see Figs. 2 and 3a) The oxygen stoichiometry of BIW phase could be checked and no deficiency was detected within the standard deviations. The most important structural parameters of the crystallographic structure and the reliability factors of the two refinements are listed in Table 1; selected angles and main bond lengths were listed in Table 2. A schematic representation of the cubic perovskite is shown as an inset in Fig. 3a.

The Goldschmith's tolerance factors (t) were calculated for these phases using the ionic radii given by Shannon [18] as $t = (r_A + r_O)/[\sqrt{2}[(2r_{B'} + r_{B''})/3 + r_O]$. The values obtained were 0.998 and 0.978 for BIW and BIU, respectively; these figures are near to that expected for the ideal cubic perovskite tolerance factor ($t = 1$). It is remarkable that other Ba-containing compounds with similar stoichiometry but with the larger B-site atom (In^{3+} or Sc^{3+}) in lower proportion, like $Ba_3Ir_2InO_9$ and $Ba_3Ir_2ScO_9$ [19], display t-values above the unity (e.g. 1.031 for $Ba_3Ir_2InO_9$), so they adopt a 6H-perovskite-type structure (S.G. $P6_3/mmc$). By contrast, in our case, the major proportion of the bigger B-site atom leads to a reduction of the Goldschmith's tolerance factor and the compounds crystallize in a cubic structure.

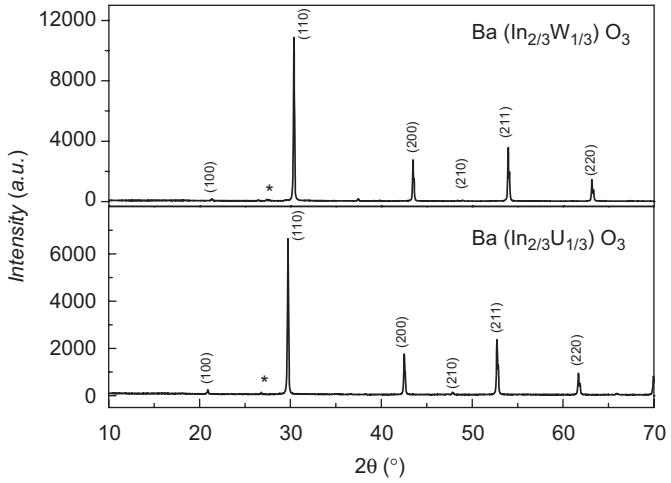

Fig. 1. XRD pattern for $Ba(In_{2/3}B''_{1/3})O_3$, indexed in a cubic unit cell. The stars correspond to the most intense reflection of $BaB''O_4$ impurity.

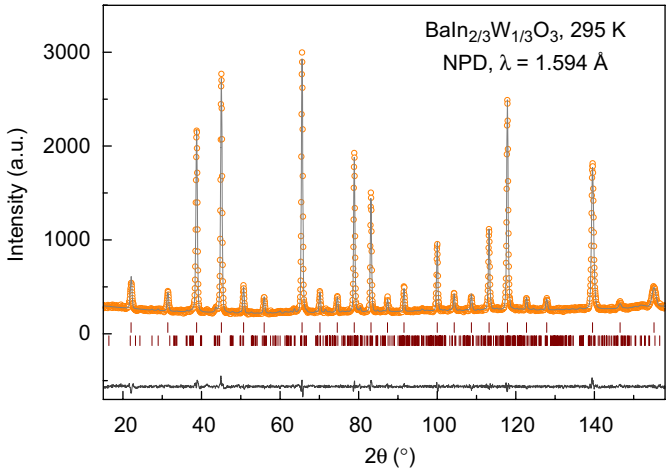

Fig. 2. NPD Rietveld profiles for $Ba(In_{2/3}W_{1/3})O_3$ at 295 K. Observed (circles), calculated (full line) and difference (bottom). The second row of tick lines represents the Bragg reflections of the impurity $BaWO_4$.

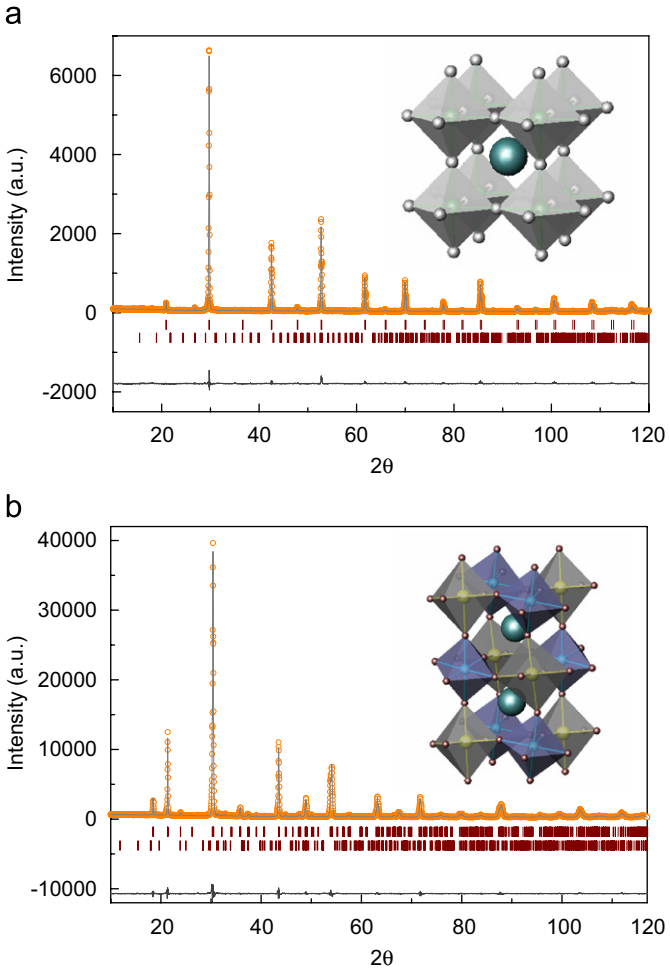

Fig. 3. (a) XRPD Rietveld profiles for $Ba(In_{2/3}U_{1/3})O_3$. Observed (circles), calculated (full line) and difference (bottom). The second row of tick lines corresponds to the Bragg reflections of the impurity $BaUO_4$. *Inset*: A view of the crystal structure of the $Ba(In_{2/3}B''_{1/3})O_3$ perovskite. Gary spheres represent the O atoms, the spheres inside the octahedra represent the (In/B'') atoms and the bigger sphere represents the Ba atom. (b) XRPD data for $Sr_3In_2UO_9$. The second row of tick lines corresponds to the Bragg reflections of the impurity $SrIn_2O_4$. *Inset*: A view of the crystal structure of $Sr_3In_2B''O_9$ perovskite. Corner spheres represent the O atoms and the bigger spheres inside the octahedra represent the In atoms at 2*d*-site, while the smaller spheres inside the octahedra represent the $(In_{1/3}B''_{2/3})$ 2*c*-site atoms and the biggest spheres represent the Sr atoms.

Table 1
Unit cell, positional and thermal parameters for $Ba(In_{2/3}B''_{1/3})O_3$ (B'' = W, U) in the cubic $Pm\bar{3}m$ space group, from NPD data for BIW and from XRPD for BIU

	B'' = U	B'' = W
$a = b = c$ (Å)	4.24941(1)	4.16111(1)
V (Å^3)	76.734(2)	72.048(2)
Ba 1b (1/2, 1/2, 1/2)		
B (Å^2)	1.00(4)	0.84(2)
In 1*a* (000)		
B (Å^2)	0.20(3)	0.51(2)
B'' 1*a* (000)		
B (Å^2)	0.20(3)	0.51(2)
O 3*d* (1/200)		
B(Å^2)	1.3 (2)	1.66 (1)
Reliability factors		
R_p (%)	17.3	11.4
R_{wp} (%)	15.0	8.5
R_{exp} (%)	19.1	7.32
χ^2	0.63	1.35
R_B (%)	6.41	1.65

Table 2
Main bond length (Å) and selected angles (°) for cubic $Ba(In_{2/3}B''_{1/3})O_3$ (B'' = W, U) determined from the NPD data for BIW and from XRD for BIU

	B'' = U	B'' = W
δBa–O (× 12)	3.00479(1)	2.94191(1)
δ(2/3In/1/3B'')–O (× 6)	2.12471(1)	2.08024(1)
α(In–O–B'')	180.00	180.00

As shown in Table 1, the unit cells parameters scale with the B'' ionic radii variation, spanning from 0.60 Å for W^{6+} to 0.73 Å^{6+}. According to this, the interatomic distance between the atoms located in two neighbouring octahedral sites is longer for the U-containing phases. The calculated Ba–O distances from the ionic radii sums, of 3.01 Å, is close to that observed for both Ba phases (see Table 2). On the other hand, the $\langle(In_{2/3}W_{1/3})–O\rangle$ calculated distance is 2.126 Å, which is in agreement with the observed value (2.08 Å); for the U-containing phase the calculated $\langle(In_{2/3}U_{1/3})–O\rangle$ distance is 2.16 Å, very close to that observed (2.12 Å).

Finally it is interesting to note that BIW previously obtained by a sol–gel route and studied by XRPD and TEM techniques [13] was identified as a mixture of two phases, 70% of a fully ordered cubic double perovskite S.G. $Pm\bar{3}m$ and 21% of the $Pm\bar{3}m$ one. In our case, after a careful refinement of the structures from NPD data, no evidence of this mixture was detected. The actual synthetic conditions by standard ceramic methods, implying thermal treatments at rather elevated temperatures, promotes the formation of an homogeneous, single phase of the fully disordered perovskite.

3.2. Sr-containing phases

The two Sr-containing phases were obtained as well-crystallized white-yellow powders, and their XRPD patterns were indexed with monoclinic symmetry. Both patterns present superstructure reflections due to the partial ordering between In and B''-site atoms.

The structural refinements for $Sr_3In_2UO_9$ from XRPD and $Sr_3In_2WO_9$ from combined NPD and XRPD data (see Fig. 3b and 4) were performed in the monoclinic $P2_1/n$ space group (No. 14), with unit cell parameters related to the ideal cubic perovskite parameter ($a_0 \approx 4$ Å as $a \approx b \approx \sqrt{2}a_0$ and $c \approx 2a_0$. As we

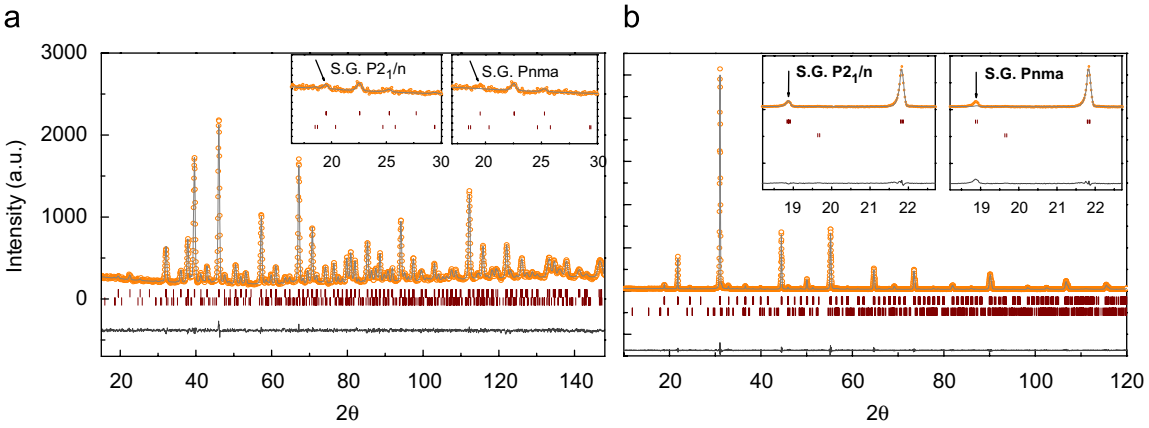

Fig. 4. Observed (circles), calculated (full line) and difference (bottom) profiles after a combined refinement for $Sr_3In_2WO_9$: (a) High-resolution NPD at 295 K fit part and (b) XRPD fit part. *Insets*: Close-ups of the superstructure peaks using $P2_1/n$ (left) and *Pnma* (right) models, respectively.

mentioned in the introduction, the crystallographic formula of these compounds could be re-written as $Sr_2In(In_{1/3}B''_{2/3})O_6$ similar to an $A_2B'B''O_6$ double perovskite. In this model it is necessary to define two crystallographically different B positions, In and In/B'', and three different oxygen atoms that are located at general positions. Therefore, the Sr atoms were located at 4*e* (*x*, *y*, *z*)-sites; In at 2*d* (1/2, 0, 0); (In/B'') at 2*c* (0, 1/2, 0), and the three kinds of oxygen atoms at the 4*e* (*x*, *y*, *z*) positions.

In order to check the results described by Fuentes et al. [13], where $Sr_3In_2WO_9$ was refined as a totally disordered orthorhombic perovskite, we carried out an alternative joint refinement (XRD and NPD data) in the *Pnma* space group, which does not admit a long-range ordering between the B atoms: in that present case the quality of the fit was considerably worse ($^{NPD}R_B = 4.28\%$; $^{XRD}R_B = 3.02\%$), leaving unexplained some superstructure reflections that appear at low angles (see insets of Figs. 4a and b). When the refinement was carried out in the monoclinic space group $P2_1/n$, which considers two crystallographically independent B-sites and thus admits long-range ordering, all the reflections were well resolved and a significantly better fit was obtained. A minor impurity of $SrIn_2O_4$ was detected and included in the refinement as a second phase. This was defined in the space group *Pnam* (No. 62) and from the scale factors, the amount of this impurity was 2.9%. Given that the difference between the neutron scattering lengths of In and W is very small (4.1 fm for In and 4.8 fm for W) the determination of the anti-site effect was very effective from the mentioned joint refinement of the SIW structure from high-resolution XRPD and NPD data, taking advantage of the larger contrast existing for XRD scattering factors. Considering that the structure with a 100% of order between the octahedral B-site atoms is $Sr_2[In]_{2d}[In_{1/3}W_{2/3}]_{2c}O_6$, the degree of B-site cations order obtained from the refined structure was 97%; accordingly the refined crystallographic formula of this compound should be re-written as $Sr_2[In_{0.97}W_{0.03}]_{2d}[In_{0.37}W_{0.63}]_{2c}O_6$. So, as a good approximation we can assume that this compound presents a full B-site atomic order.

For the uranium-containing sample $Sr_3In_2UO_9$ (SIU) the structural refinement was carried out from XRPD data, and a good fit was also obtained using the $P2_1/n$ model (Fig. 3b). A minor $SrIn_2O_4$ impurity was detected and included in the refinement; from the scale factors its amount is 2.2%. The most important structural parameters and the reliability factors after the final refinements are listed in Table 3; selected angles and main bond lengths are listed in Table 4. SIU shows a totally ordered structure, containing alternating InO_6 and $(In_{1/3}U_{2/3})O_6$ octahedra, which exhibit an in-phase octahedral tilting along the (001) direction of the pseudo-cubic cell, and antiphase tiltings along the (010) and (100) directions (Fig. 5), which corresponds to the $a^-a^-b^+$ system according to the Glazer notation for the $P2_1/n$ double perovskite structures as derived by Woodward [20].

In this case the unit-cell parameters and positions are quite different for the W and U perovskites, due to the ionic size difference between W^{6+} and U^{6+} cations. The U phase exhibits a larger monoclinic distortion than the W oxide. This fact is reasonable since the calculated Goldschmith's tolerance factors are $t = 0.923$ for SIU and $t = 0.942$ for SIW. The average tilting angle for these two compounds can be estimated by $\theta = (180 - \Psi)/2$ where $\Psi = \langle \text{In–O–(In}_{1/3}B''_{2/3})\rangle$. For $B'' = U$ we obtain $\theta = 13^\circ$, whereas for $B'' = W$ the tilting angle is lower, taking the value of 11.2° as expected from the larger tolerance factor. A view of the monoclinic perovskite structure is displayed in Fig. 5.

In the rather distorted SrO_{12} polyhedron the effective coordination of Sr cations can be considered as eightfold (disregarding distances longer than 3 Å) with average $\langle \text{Sr–O}\rangle_{\text{short}}$ of 2.704 and 2.736 Å for SIW and SIU, respectively. These values are in reasonable agreement with those expected from the ionic radii sums [18] of 2.66 Å for $^{VIII}Sr^{2+}$ (i.r.: 1.26 Å) and $^{VI}O^{2-}$ (i.r.: 1.40 Å). For SIW, the average $\langle (In/W)_{2d}–O_3\rangle$ and $\langle (In/W)_{2c}–O_3\rangle$ observed distances are also close to the calculated values from the ionic radii sums, taking into account the occupancy factors for each site, of 2.194 and 2.07 Å, respectively. In the case of SIU, the In^{3+} cations fully occupy the 2*d*-site with an average distance $\langle (In)_{2d}–O_3\rangle$ of 2.16 Å, which is close to the calculated value (2.20 Å), while for the 2*c* octahedral site, the average and the calculated distance were 2.13 and 2.153 Å, respectively.

A final remark concerns the differences observed between the Ba and Sr compounds: a surprising result is the absence of superstructure peaks for the Ba perovskites, implying a total anti-site disordering between both B cations, even though the difference in charge between them is of three valence units; in general, it has been observed that long-range ordering between B cations is established for valence differences larger than two. If we analyse the combined influence of the charge and the ionic radii difference between two hypothetically different B-sites, $(In)_{site1}$ and $(In_{1/3}W_{2/3})_{site2}$, which is the highest degree of ordering that this composition can admit, we notice that the charge difference between the two sites is 2 ($[3]_{site\ 1}$–$[5]_{site\ 2}$) and the ionic radii difference is $\Delta r = 0.14$ Å; according to these two factors and following the order criterion proposed by Anderson et al. [21], these phases should be ordered. In our case the two A = Ba phases are fully disordered whereas for $A = Sr$ they exhibit total long-range ordering, and this fact is certainly related to the *A*/*B* size ratio. As a general fact, the cationic disorder over the B positions in double perovskites generates regions where sets of adjacent

Table 3
Unit cell, positional and thermal parameters for $Sr_3In_2B''O_9$ ($B'' = W, U$) in the monoclinic $P2_1/n$ space group, from NPD/XRPD data for SIW and from XRPD for SIU

	Sr_2 [In]$_{2d}$[$In_{1/3}U_{2/3}$]$_{2c}O_6$	Sr_2 [$In_{0.97}W_{0.03}$]$_{2d}$[$In_{0.37}W_{0.63}$]$_{2c}O_6$
a (Å)	5.861(1)	5.7548(2)
b (Å)	5.908(1)	5.7706(2)
c (Å)	8.315(2)	8.1432(3)
β (°)	89.98(1)	90.01(1)
V (Å^3)	287.9(1)	270.42(1)
Sr 4*e*(*xyz*)		
x	0.511(1)	0.507(7)
y	0.532(2)	0.526(4)
Z	0.250(2)	0.248(1)
B (Å^2)	1.80(5)	0.81(4)
In 2*d*(1/200)		
B(Å^2)	0.34(5)	0.2(1)
Occ	0.99(2)	0.97(1)
B'' 2*d*(1/200)		
B(Å^2)	0.34(5)	0.2(1)
Occ	0.01(2)	0.03(1)
In 2*c*(01/20)		
B (Å^2)	0.18(3)	0.1(1)
Occ	0.34(2)	0.37(1)
B'' 2*c*(01/20)		
B (Å^{-2})	0.18(3)	0.1(1)
Occ	0.65(2)	0.63(1)
O1 4*e*(*xyz*)		
x	0.218(4)	0.207(2)
y	0.202(4)	0.229(1)
z	0.967(5)	0.963(1)
B (Å^2)	1.00	1.8(2)
O2 4^e(*xyz*)		
x	0.300(4)	0.280(2)
y	0.706(4)	0.702(1)
z	0.948(5)	0.967(1)
B (Å^2)	1.00	0.7(1)
O(3) 4*e*(*xyz*)		
x	0.426(3)	0.433(1)
y	0.988(3)	0.984(1)
z	0.261(4)	0.259(2)
B (Å^2)	1.00	1.1(1)
Reliability factors		
NPD		
R_p (%)	–	12.2
R_{wp} (%)	–	11.2
R_{exp} (%)	–	9.02
χ^2	–	1.54
R_B (%)	–	2.53
XRD		
R_p (%)	12.2	13.7
R_{wp} (%)	12.8	12.9
R_{exp} (%)	6.85	15.2
χ^2	3.62	0.72
R_B (%)	3.20	2.12
	Global χ^2 for the joint refinement: 1.13	

highly charged cations (for instance W^{6+} or U^{6+}) give rise to an electrostatic repulsion that promotes the long-range ordering, which is realized if the temperature is sufficiently high to permit the cationic motion. For the particular composition $A(In_{2/3}B''_{1/3})O_3$, the repulsion between highly charged B'' cations is partially shielded by the double contents of In^{3+} cations, in such a way that the mentioned electrostatic driving force for long-range ordering becomes only apparent when the distances between B cations is sufficiently small. Here the size of the A cation is of paramount importance, since it determines the size of the unit-cell and therefore the B–B distances (B-sites being at special positions): for

Table 4
Main interatomic distances (Å) and angles (°) for $Sr_3In_2B''O_9$ ($B'' = W, U$) in the monoclinic $P2_1/n$ space group from combined NPD/XRPD data for SIW and from XRPD for SIU

	Sr_2 [In]$_{2d}$ [$In_{1/3}U_{2/3}$]$_{2c}O_6$	Sr_2 [$In_{0.97}W_{0.03}$]$_{2d}$[$In_{0.37}W_{0.63}$]$_{2c}O_6$
SrO_{12} Polyhedra		
Sr–O_1	3.49(3)[a]	3.366(15)[a]
Sr–O_1	2.88(4)	2.909(16)
Sr–O_1	2.87(3)	2.760(14)
Sr–O_1	2.58(3)	2.559(14)
Sr–O_2	2.98(4)	2.824(15)
Sr–O_2	3.65(3)[a]	3.412(14)[a]
Sr–O_2	2.43(3)	2.507(14)
Sr–O_2	2.83(3)	2.846(13)
Sr–O_3	3.25(2)[a]	3.162(5)[a]
Sr–O_3	2.74(2)	2.676(5)
Sr–O_3	2.58(2)	2.550(9)
Sr–O_3	3.31(2)[a]	3.227(9)[a]
⟨Sr–O⟩$_{short}$	**2.74**	**2.704**
$(In/B'')_{2d}O_6$ Octahedra		
$(In/B'')_{2d}$–O_1 (×2)	2.09(2)	2.162(5)
$(In/B'')_{2d}$–O_2 (×2)	2.14(2)	2.151(9)
$(In/B'')_{2d}$–O_3 (×2)	2.21(3)	2.144(5)
⟨$(In/B'')_{2d}$–O_3⟩	**2.16**	**2.152**
$(In/B'')_{2c}O_6$ Octahedra		
$(In/B'')_{2c}$–O_1 (×2)	2.19(2)	1.99(1)
$(In/B'')_{2c}$–O_2 (×2)	2.18(2)	2.01(1)
$(In/B'')_{2c}$–O_3 (×2)	2.03(3)	2.00(1)
⟨$(In/B'')_{2c}$–O_3⟩	**2.13**	**2.01**
Angles around O		
$(In/B'')_{2d}$–O_1–$(In/B'')_{2c}$	156.9(3)	157.6(2)
$(In/B'')_{2d}$–O_2–$(In/B'')_{2c}$	148.8(3)	157.5(2)
$(In/B'')_{2d}$–O_3–$(In/B'')_{2c}$	156.1(4)	157.4(2)
⟨$(In/B'')_{2d}$–O–$(In/B'')_{2c}$⟩	**153.9**	**157.5**

Bold denotes the average values of the interatomic distances.
[a] Distance disregarded.

the Sr compounds, the B–B bond lengths are sizably smaller (e.g. 4.07 Å for SIW) than those observed in the corresponding Ba compounds (e.g. 4.16 Å for BIW), thus explaining that the Sr phases exhibit long-range ordering, whereas in the Ba perovskites the B''–B'' electrostatic repulsions do not become operational.

4. Conclusion

The synthesis and crystal structure of a new uranium-based double perovskite oxide $Sr_3In_2UO_9$ have been reported by first time from XRPD data, and the true symmetry of $Ba(In_{2/3}W_{1/3})O_3$, $(Ba(In_{2/3}U_{1/3})O_3)$ and $Sr_3In_2WO_9$ have been re-evaluated from NPD and XRPD data. The two barium compounds crystallise in a cubic symmetry (S.G. $Pm\bar{3}m$), showing a random distribution over the B-sites in a simple cubic aristotype perovskite unit-cell. By contrast, the Sr-containing materials are isostructural double perovskites with monoclinic symmetry (S.G. $P2_1/n$) presenting a high degree of long-range ordering (97% for SIW and 100% for SIU). The octahedral framework is fairly tilted, with average tilt angles of 11.2° and 13.0° for SIW and SIU, respectively. The presence of long-range ordering in the Sr samples, by contrast with the Ba perovskites, is related with the smaller unit cell and B–B distances in the Sr oxides, promoting the electrostatic repulsions between highly charged W^{6+} and U^{6+} cations as driving force for the long-range B-site ordering.

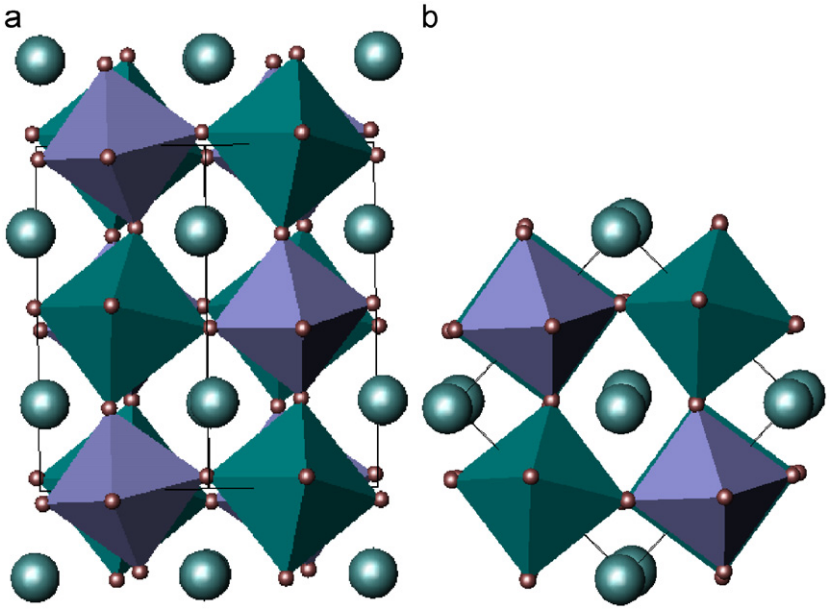

Fig. 5. A projected view of $Sr_3In_2B''O_9$ (B'' = W or U) along (a) (100) plane and (b) (001) plane. The antiphase (−) tilting around [100] and the in-phase tilting around [001] of the adjacent octahedral layers can clearly be seen.

Acknowledgments

S.A.L. thanks a CONICET fellowship. J.C.P. thanks CONICET (Project PIP no. 6246), SECyT-UNSL (Project 7707) and ANPCYT (Project PICT 25459). J.C.P. is member of CONICET. J.A.A. acknowledges the financial support of the Spanish Ministry of Education to the project MAT2007-60536. We are grateful to I.L.L. for making all facilities available.

References

[1] K.I. Kobayashi, T. Kimura, H. Sawada, K. Terakura, Y. Tokura, Nature (London) 395 (1998) 677.
[2] R.V.K. Mangalam, P. Mandal, E. Suard, A. Sundaresan, Chem. Mater. 19 (2007) 4114.
[3] Naohisa Takesue, Yasuhiko Fujii, Masaki Ichihara, Haydn Chen, Phys. Rev. Lett. 82 (1999) 3709.
[4] Masaki Azuma, Kazuhide Takata, Takashi Saito, Shintaro Ishiwata, Yuichi Shimakawa, Mikio Takano, J. Am. Chem. Soc. 127 (2005) 8889.
[5] C. Ritter, M.R. Ibarra, L. Morellón, J. Blasco, J. García, J.M. De Teresa, J. Phys.: Condens. Matter 12 (2000) 8295.
[6] M.C. Viola, M.S. Ausburger, R.M. Pinacca, J.C. Pedregosa, R.E. Carbonio, R.C. Mercader, J. Solid State Chem. 175 (2003) 252.
[7] C. Viola, J.A. Alonso, J.C. Pedregosa, R.E. Carbonio, Eur. J. Inorg. Chem. (2005) 1559.
[8] R.M. Pinacca, M.C. Viola, J.C. Pedregosa, R.E. Carbonio, J.A. Alonso, J. Mater. Chem. 15 (2005) 4648.
[9] M.S. Augsburger, M.C. Viola, J.C. Pedregosa, R.E. Carbonio, J.A. Alonso, J. Mater. Chem. (RSC) 16 (2006) 4235.
[10] F. Galasso, L. Katz, R. Ward, J. Am. Chem. Soc. 81 (1959) 820.
[11] F. Galasso, W. Darby, J. Phys. Chem. 66 (1962) 131.
[12] R. Liu, Y. Xuan, Y.Q. Jia, Mat. Chem. Phys. 57 (1998) 81.
[13] Antonio F. Fuentes, O. Hernández-Ibarra, G. Mendoza-Suarez, J.I. Escalante-García, Khalid Boulahya, U. Amador, J. Solid State Chem. 173 (2003) 319.
[14] W.T. Fu, D.J.W. IJdo, Solid State Commun. 134 (2005) 177.
[15] V. Ting, Y. Liu, R.L. Withers, E. Krausz, J. Solid State Chem. 177 (2004) 979.
[16] J. Berthon, J.C. Grenet, P. Poix, Ann. de Chim. (Paris) (1979) 609.
[17] J. Rodríguez-Carvajal, Physica B 192 (1993) 55.
[18] R.D. Shannon, Acta Crystallogr. Sect. A 32 (1976) 751.
[19] Takeshi Sakamoto, Yoshihiro Doi, Yukio Hinatsu, J. Solid State Chem. 179 (2006) 2595.
[20] P.M. Woodward, Acta Crystallogr. Sect. B 53 (1997) 32.
[21] M.T. Anderson, K.B. Greenwood, G.A. Taylor, K.R. Poeppelmeier, Prog. Solid State Chem. 22 (1993) 197.